

Tapering in the wavefield extrapolation

Kun Liu, Hugh D. Geiger, and John C. Bancroft

ABSTRACT

Recursive Kirchhoff extrapolation has attractive merits that make it an ideal candidate for implementation in pre-stack depth migrations. However, the artifacts resulting from data and operator aperture truncations may cause instability and inaccuracy. Tapering is widely recognized as an effective tool to deal with truncation problems. In wavefield extrapolation, the conventional method is to apply a taper to the data edges and then extrapolate the tapered data with a tapered extrapolator. However, as we show in this paper, this method may result in a loss of accuracy, especially for the first-step of wavefield extrapolation where the input surface data are usually zero-padded to the extent of the migration aperture. We introduce an adaptive tapering scheme that varies with output locations and handles both truncations dynamically. Synthetic examples show that the extrapolation with adaptive tapering achieves a better accuracy than conventional separate application of data tapering and operator tapering.

INTRODUCTION

Recursive wavefield extrapolation is an essential component of one-way approaches to ‘wave equation’ imaging (c.f., Berkhout, 1981). These approaches have found wide application in recent years as computational power has steadily increased and as exploration efforts target areas with strong lateral variations in seismic velocity. These one-way recursive extrapolators can deal with complex wave phenomena such as multiple arrivals and complicated scattering more easily than nonrecursive Kirchhoff (i.e. diffraction stack) methods.

Many algorithms have been developed that fall into the general category of recursive wavefield extrapolation, including finite-difference (Claerbout, 1985), space-frequency extrapolation (Berkhout, 1981), phase-shift-plus-interpolation (Gazdag and Sguazero, 1984), split-step Fourier (Stoffa et al., 1989), nonstationary phase shift (Margrave and Ferguson, 1999; Ferguson and Margrave, 2002), and recursive Kirchhoff (Bevc, 1997; Margrave and Daley, 2001; Geiger et al., 2002). There are two main types of extrapolation methods, explicit and implicit. Recursive Kirchhoff extrapolation, the focus of this paper, is an explicit extrapolation method that is implemented as a convolutional filter in the space-frequency domain. Like other explicit extrapolation schemes, it is conceptually simple in both 2-D and 3-D, and can be efficiently coded for implementation on parallel clusters (Geiger et al., 2002). Moreover, it combines the best features of nonrecursive Kirchhoff methods and Fourier wavefield extrapolation as it can accommodate irregular acquisition geometries with reasonable computational efficiency (Margrave and Daley, 2001).

Despite the mentioned advantages, stability and accuracy are always big concerns when designing explicit recursive Kirchhoff extrapolators. Unlike implicit methods which are guaranteed to be stable (Claerbout, 1985), explicit methods tend to be numerically unstable (Hale, 1991; Etgen, 1994). In most cases, the instability and

inaccuracy are caused by the truncation of the extrapolator to a finite aperture (Nautiyal, 1993). Generally, there are two kinds of aperture truncations. The first kind occurs because the field data are always truncated at the bounds of the recorded survey. The second kind arises because the ideal infinite spatial extent of the extrapolation operator must be truncated to a finite size to achieve computational efficiency.

The standard method for handling a finite survey aperture is to apply tapers to the data edges prior to extrapolation. A proper handling of the data edges is especially important for the first extrapolation step where the input surface data are typically padded with zero traces out to the desired size of the migration aperture. However, it is still not clear if this static tapering is necessary, as it may introduce additional inaccuracies (Claerbout, 1985). The typical remedy for extrapolator truncation is to apply a taper to the extrapolator (e.g., Nautiyal et al., 1993). Given these concerns, we are motivated to develop an “adaptive” taper that handles both the finite survey aperture (with zero padding) and the finite spatial extent of extrapolator operator.

In this paper, we briefly review the theory of recursive Kirchhoff extrapolation. Then, we focus our investigation on the initial step of the wavefield extrapolation where the input data are zero padded. A simple synthetic test is used to differentiate the artifacts arising from data truncation and extrapolator truncation. Next, we introduce an adaptive tapering scheme that minimizes both kinds of truncation artifacts. The adaptive taper is integrated into the extrapolator algorithm and varies depending on the location of the output point. Thus, it is not necessary to taper the data prior to extrapolation. Tests using the synthetic data suggest that the adaptive taper reduces artifacts compared with the traditional combination of a data taper plus extrapolator taper.

THEORY REVIEW: RECURSIVE KIRCHHOFF EXTRAPOLATION

If $\psi(x, y, z = 0, \omega)$ is a wavefield in the space-frequency (x, y, ω) domain at depth level $z = 0$, then its extrapolated value at depth z is calculated as

$$\psi(x, y, z, \omega) = \int_{-\infty}^{\infty} \psi(\hat{x}, \hat{y}, z = 0, \omega) W_{3D}(x - \hat{x}, y - \hat{y}, z, v, \omega) d\hat{x}d\hat{y}, \quad (1)$$

where v is the laterally variable velocity and W_{3D} is the three-dimensional, space-frequency, wavefield extrapolation operator. It can be derived by taking the z derivative of 3-D Green’s function for constant velocity, i.e.

$$W_{3D}(x, y, z, v, \omega) = -2 \frac{\partial}{\partial z} g_{3D}(x, y, z, v, \omega) = -\frac{ik \cos \theta}{2\pi r} e^{ikr} \left(1 + \frac{i}{kr}\right), \quad (2)$$

where $r = \sqrt{x^2 + y^2 + z^2}$, $k = \frac{\omega}{v}$ and $\cos \theta = \frac{z}{r}$ is the cosine of the scattering angle.

By substituting equation (2) into equation (1), we obtain

$$\psi(x, y, z, \omega) = \frac{-i\omega}{2\pi} \int_{-\infty}^{\infty} \psi(\hat{x}, \hat{y}, z=0, \omega) \frac{z}{v\tilde{r}^2} e^{i\omega\tilde{r}/v} \left(1 + \frac{iv}{\omega\tilde{r}}\right) d\hat{x}d\hat{y}, \quad (3)$$

where $\tilde{r} = \sqrt{(x - \hat{x})^2 + (y - \hat{y})^2 + z^2}$. Equation (3) is a spatial convolution of the wavefield with an operator that performs a weighted summation along a diffraction curve. Therefore, equation (3) is interpretable as a Kirchhoff-style wavefield extrapolation operation in the space-frequency domain (Margrave and Daley, 2001). Depending on the choice of Fourier transform convention, W_{3D} can represent either a forward or backward wavefield extrapolation operator.

Similarly, 2-D wavefield extrapolation is given by

$$\psi(x, z, \omega) = \int_{-\infty}^{\infty} \psi(\hat{x}, z=0, \omega) W_{2D}(x - \hat{x}, z, v, \omega) d\hat{x}. \quad (4)$$

The 2-D wavefield extrapolation operator W_{2D} can be derived by taking the z derivative of 2-D Green's function, i.e.

$$W_{2D}(x, z, v, \omega) = -2 \frac{\partial}{\partial z} g_{2D}(x, z, v, \omega) = -\frac{i}{2} \frac{\partial H_0^{(1)}(k\rho)}{\partial z}, \quad (5)$$

where $\rho = \sqrt{x^2 + z^2}$ and $H_0^{(1)}(u)$ is the zero-order Hankel function of the first kind. For numerical calculation, the derivative of $H_0^{(1)}(u)$ can be deduced as

$$\frac{\partial}{\partial u} [H_0^{(1)}(u)] = -H_1^{(1)}(u) = -[J_1(u) + iY_1(u)], \quad (6)$$

where $J_1(u)$ and $Y_1(u)$ are the first-order Bessel function of the first kind and second kind, respectively. Standard routines for calculating $J_1(u)$ and $Y_1(u)$ can be found in the published literature (e.g., Press, 1992). Plugging equation (6) into equation (5), the 2-D extrapolation operator for constant velocity becomes

$$W_{2D}(x, z, v, \omega) = \frac{i\omega \cos \theta}{2v} H_1^{(1)}\left(\frac{\omega\rho}{v}\right), \quad (7)$$

where $\cos \theta = \frac{z}{\rho}$ is the cosine of the scattering angle.

A final form for 2-D extrapolator can be developed by substituting equation (7) into equation (4), yielding

$$\psi(x, z, \omega) = \frac{i\omega}{2} \int_{-\infty}^{\infty} \psi(\hat{x}, z=0, \omega) \frac{\cos \theta}{v} H_1^{(1)}\left(\frac{\omega \tilde{\rho}}{v}\right) d\hat{x}, \quad (8)$$

where $\tilde{\rho} = \sqrt{(x - \hat{x})^2 + z^2}$. Equation (8) is a 2-D convolution filter that can represent either forward or backward extrapolation, depending on the choice of Fourier transform convention.

The simple replacement of constant velocity by lateral variable velocity in equation (3) and (8) leads to the extrapolators that can approximately accommodate lateral velocity variations. For example, the 2-D and 3-D Kirchhoff GPSPI extrapolators are given by

$$\psi_{2D}^{PSPI}(x, z, \omega) = \frac{i\omega}{2v(x)} \int_{-\infty}^{\infty} \psi(\hat{x}, z=0, \omega) \frac{z}{\tilde{\rho}} H_1^{(1)}\left(\frac{\omega \tilde{\rho}}{v(x)}\right) d\hat{x}, \quad (9)$$

$$\psi_{3D}^{PSPI}(x, y, z, \omega) = \frac{-i\omega}{2\pi v(x, y)} \int_{-\infty}^{\infty} \int_{-\infty}^{\infty} \psi(\hat{x}, \hat{y}, z=0, \omega) \frac{z}{\tilde{r}^2} e^{i\omega \tilde{r}/v(x, y)} \left(1 + \frac{iv(x, y)}{\omega \tilde{r}}\right) d\hat{x} d\hat{y}, \quad (10)$$

where $v(x)$ and $v(x, y)$ are the velocities at the output point.

TAPERING IN THE WAVEFIELD EXTRAPOLATION

In the real world, the ideal infinite integral in the extrapolator can only be approximated by finite summation, either because our acquisition survey is always limited to some extent or because we want to confine the summation aperture to reduce the computational cost. It is widely agreed that the abrupt truncations in the wavefield extrapolation result in artifacts that cause both instability and inaccuracy (e.g., Nautiyal et al., 1993; Etgen, 1994). For the initial extrapolation where the input wavefield at $z=0$ is padded with zero traces, more efforts should be devoted to handle the truncations. Otherwise, errors that occur in the first step of the extrapolation tend to accumulate with subsequent applications of the recursive operator. A simple 2-D synthetic test can be used to show the truncation artifacts arising with the first extrapolation step.

Figure 1 is the synthetic input section that consists of three dipping events, with $dx=18m$, and $dt=4ms$. For this test, a constant velocity of 2000m/s is assumed for convenience, but the general results are also applicable to variable velocity. Before extrapolation the data are padded with null traces at the edges so that events can be extrapolated beyond the original extent of the survey. The angular aperture of the extrapolator is limited to 70 degrees, which is equivalent to setting a maximum scattering angle ($\theta = \cos^{-1}(z/r)$) of 70 degrees. The input wavefield is then upward extrapolated with a single depth step of 200m. Figure 2 shows the output wavefield with no data or extrapolator tapers. The two kinds of truncation artifacts are readily apparent: artifacts "1" are from the data truncation and artifacts "2" are due to extrapolator truncation. In Figure 3, the extrapolation operator is the same as in Figure 2, but includes a 17.5-degree Hanning taper out to 87.5 degrees. The artifacts caused by the extrapolator truncation are almost completely removed but the artifacts caused by the data truncation are still present. The conventional approach to reducing artifacts from data truncation is to apply an edge taper to the data. However, this kind of static data tapering may cause unnecessary

accuracy losses, as the data would be double-tapered by both data and extrapolator tapers when the extrapolation operator reaches the edge of the data. Thus, we are motivated to design an adaptive tapering scheme that can dynamically handle the data and extrapolator truncations with minimal loss of accuracy.

Figure 4 illustrates how the extrapolation operator incorporates an adaptive taper that varies with output location. The percent ratio of the taper angle to the maximum scattering angle is the key parameter that controls both the taper of the operator aperture and the taper of the data aperture. To implement the adaptive taper, the output locations are divided into three zones: the left padding zone, the data zone, and the right padding zone, corresponding to MH , HI and IN in Figure 4. When the output point O_1 lies in the left padding zone (MH), the taper scheme is as shown in Figure 4(b). The angle BO_1C and DO_1E are responsible for taper control and chosen such that they have the same percentage of angle KO_1B and θ (e.g., $\angle BO_1C = 0.25 \times \angle KO_1B$ and $\angle DO_1E = 0.25 \times \theta$). Once the taper zones (BC and DE) are determined, the tapers can be immediately calculated and applied to the input wavefield; When the output point O_2 lies in the data zone (HI in Figure 4(c)), the angle $B'O_2C$ and DO_2E are chosen to be the same percentage of angle θ . Thus, taper zones $B'C$ and DE can be identified similar to when the output point O_3 lies in the right padding zone (IN in Figure 4(d)), except that the sign of the angle is negative. Here we only showed the tapering scheme for the initial extrapolation, but the tapering scheme as described for the data zone can be applied in subsequent extrapolation steps.

Figure 5 and Figure 6 provide a comparison between the extrapolation using traditional data taper plus extrapolator taper scheme and the extrapolation using the adaptive taper. The wavefield in Figure 5 is obtained by first tapering the synthetic section (Figure 1) at the data edges, and then extrapolating with the same maximum scattering angle and taper angle used in Figure 3 ($70^\circ + 17.5^\circ$). Although some artifacts are attenuated as compared to Figure 3, the data truncation artifacts are still observable, and strongest from the dipping events. The artifacts can be reduced by increasing the length of the data taper, but the price is a loss of accuracy in the extrapolated wavefield. In comparison, extrapolation using the adaptive taper (Figure 6) better attenuates the artifacts with less loss of accuracy in the extrapolated wavefield.

CONCLUSIONS

Wavefield extrapolation by recursive Kirchhoff method is attractive because it offers the possibility of combining the best features of nonrecursive Kirchhoff or diffraction stack methods (i.e., it can accommodate irregular acquisition geometries) with the increased accuracy of 'wave-equation' methods in areas with strong lateral velocity variations. As an explicit method, however, the recursive Kirchhoff method can suffer from instability and inaccuracy. Some of these errors are introduced by finite survey size and finite operator extent. Both sources of error can be reduced by intelligent application of tapers. The conventional approach is to taper the data and the extrapolator separately. However, as we show in our synthetic examples, the combination of data tapering and extrapolator tapering is not optimal, especially for the initial extrapolation step where the input surface data at $z=0$ is zero-padded out to the desired migration aperture. An adaptive taper that varies with output locations can be designed to dynamically handle

both kinds of truncations, with improved accuracy compared with the conventional approach.

FUTURE WORK

In the coming months we will apply the recursive Kirchhoff extrapolator with adaptive taper to the complex synthetic dataset (e.g., Marmousi and Sigsbee) and field data. Meanwhile, the corresponding C programs are also being developed for parallel computation.

ACKNOWLEDGEMENTS

The authors would like to thank sponsors of CREWES Project for the financial support.

REFERENCES

- Berkhout, A. J., 1981, Wave field extrapolation techniques in seismic migration, a tutorial: *Geophysics*, **46**, 1638-1656.
- Bevc, D., 1997, Imaging complex structures with semirecursive Kirchhoff migration: *Geophysics*, **62**, 577-588.
- Claerbout, J. F., 1985. *Imaging the earth's interior*: Blackwell Scientific Publications, Inc.
- Etgen, J. T., 1994, Stability of explicit depth extrapolation through laterally-varying media: 64th Annual Internat. Mtg., Soc. of Expl. Geophys., Expanded Abstracts, 1266-1269.
- Ferguson, R. J. and Margrave, G. F., 2002, Prestack depth imaging by symmetric nonstationary phase shift: *Geophysics*, **67**, 594-603.
- Gazdag, J. and Sguazero, P., 1984, Migration of seismic data by phase shift plus interpolation: *Geophysics*, **49**, 124-131.
- Geiger, H. D., Margrave G. F., Foltinek, D. S. and Langlois, J. M., 2002, Parallel 3D prestack depth migration using recursive Kirchhoff extrapolation: CREWES Research Report, **14**, 1-20.
- Hale, D., 1991, Stable explicit depth extrapolation of seismic wavefields: *Geophysics*, **56**, 1770-1777.
- Margrave, G. F. and Ferguson, R. J., 1999, Wavefield extrapolation by nonstationary phase shift: *Geophysics*, **64**, 1067-1078.
- Margrave, G. F. and Daley P. F., 2001, Recursive Kirchhoff extrapolators: CREWES Research Report, **13**, 617-646.
- Nautiyal, A., Gray, S. H., Whitmore, N. D. and Garing, J. D., 1993, Stability versus accuracy for an explicit wavefield extrapolation operator: *Geophysics*, **58**, 277-283.
- Press W. H., Teukolsky, S. A., Vetterling, W. T. and Flannery B. P., 1992, *Numerical recipes in C*: Cambridge Univ. Press.
- Stoffa, P. L., Fokkema, J. T., de Luna Freire, R. M., and Kessinger, W. P., 1990, Split-step Fourier migration: *Geophysics*, **55**, 410-421.

FIGURES

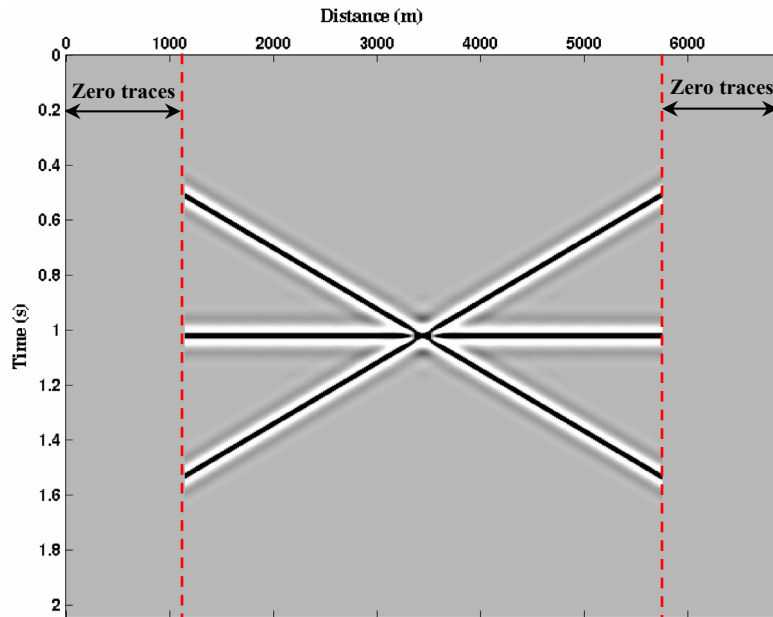


FIG. 1. Synthetic section padded with zero traces on each side. A constant velocity of 2000m/s is assumed for convenient discussion.

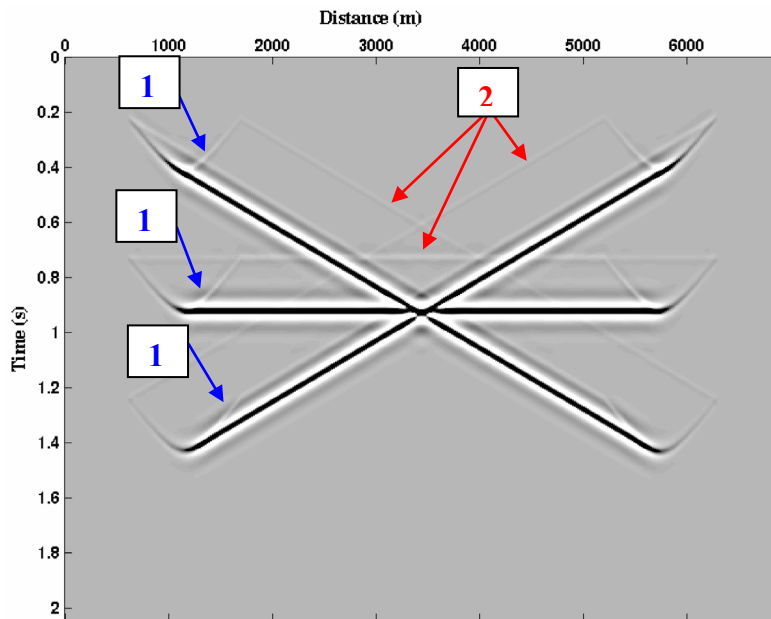


FIG. 2. The wavefield in Figure 1 is upward extrapolated using a Kirchhoff extrapolator. A single depth step of 200m is taken. Without any treatment of the truncations, artifacts occur on the output section as indicated by arrows "1" (from data truncation) and arrows "2" (from extrapolator truncation).

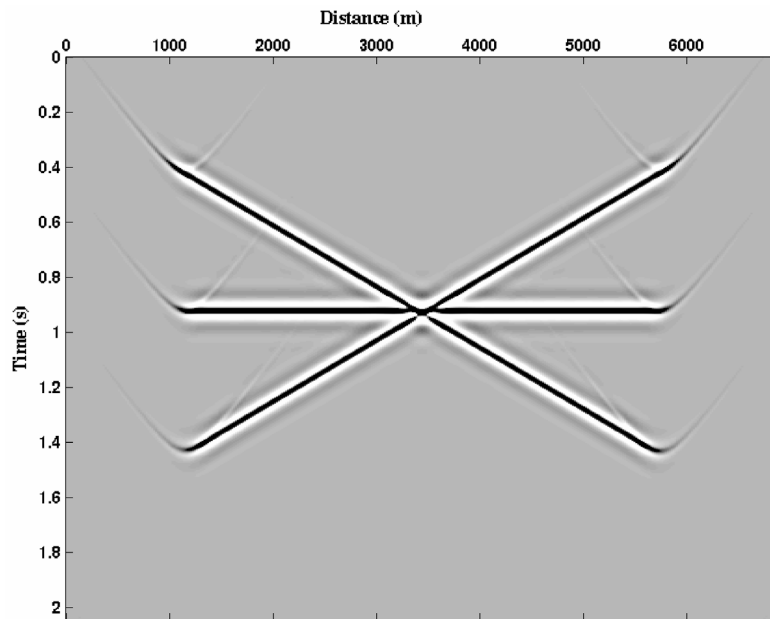


FIG. 3. The same extrapolation step as in Figure 2 except that an extrapolator taper (Hanning window) has been used. The artifacts caused by extrapolator truncation are almost removed by the taper, whereas the artifacts caused by data truncation are still present.

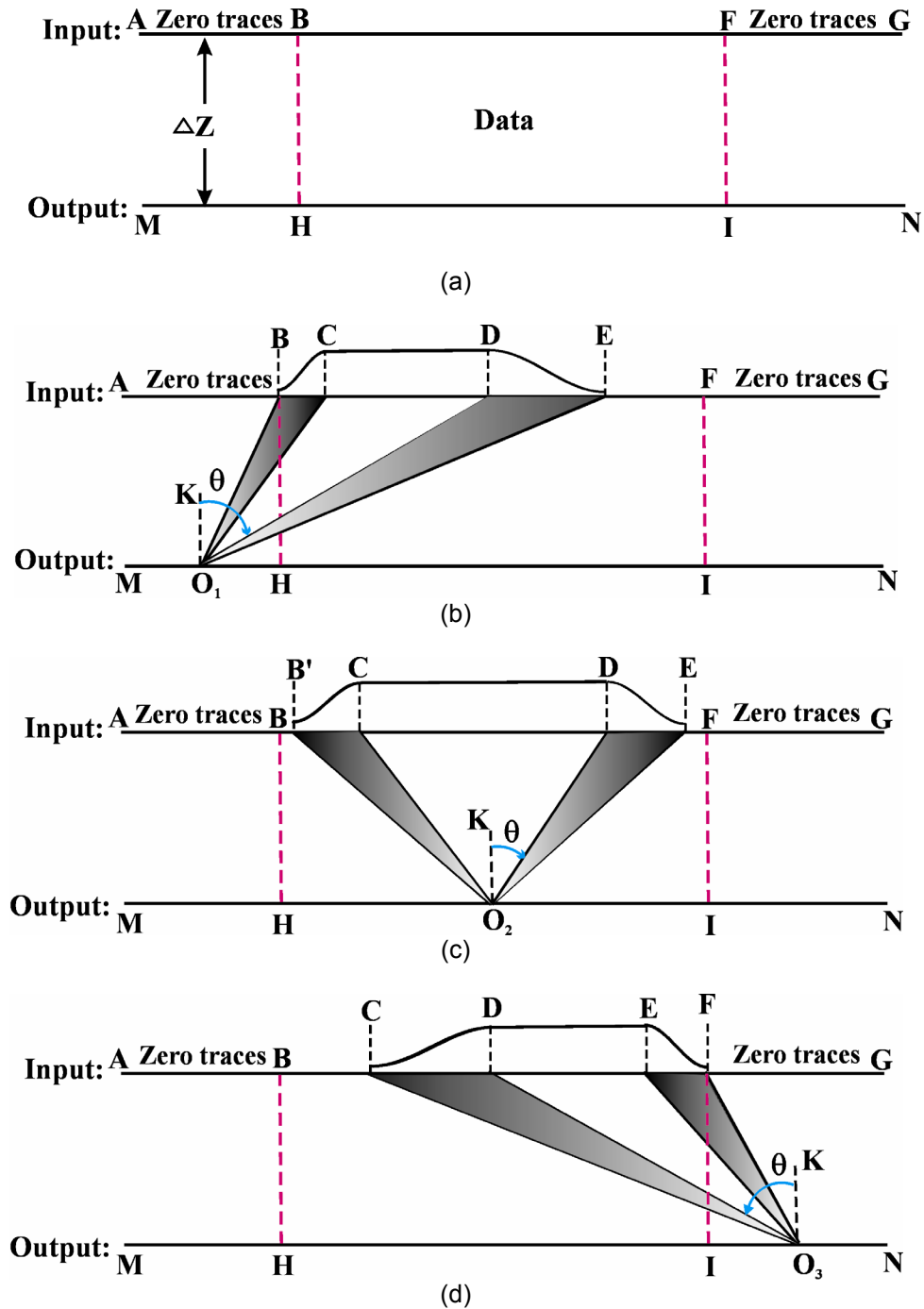


FIG. 4. The adaptive tapering schemes. The maximum scattering angle θ and taper angle are used to control the extrapolator taper. Their ratio controls the data taper when the maximum scattering angle is less than θ . (a) The surface data ($z=0$) padded with zero traces (AB and FG) are extrapolated in a depth step of Δz ; (b) The design of tapers (BC and DE) when output point O_1 lies in the left padding zone (MH); (c) The design of tapers ($B'C$ and DE) when output point O_2 lies in the data zone (HI); (d) The design of tapers (CD and EF) when output point O_3 lies in the right padding zone (IN).

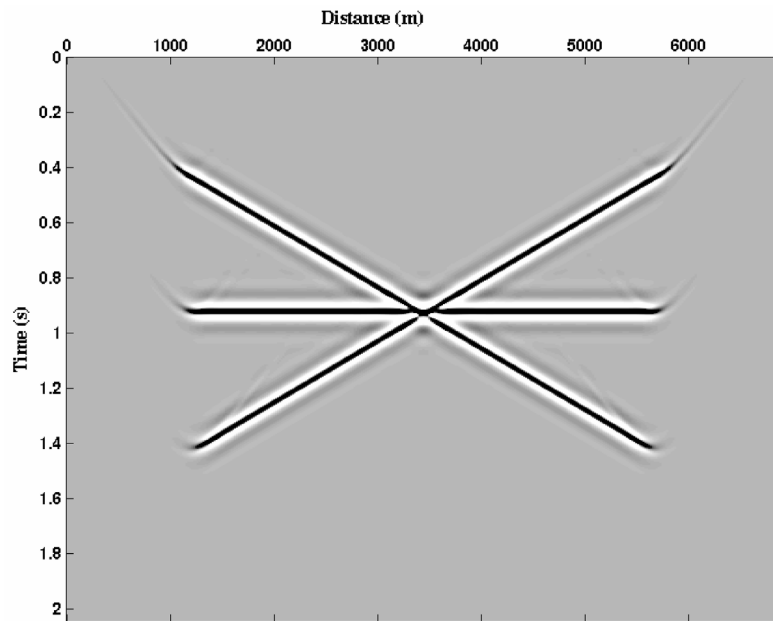


FIG. 5. Conventional extrapolation with separate data and extrapolator tapers.

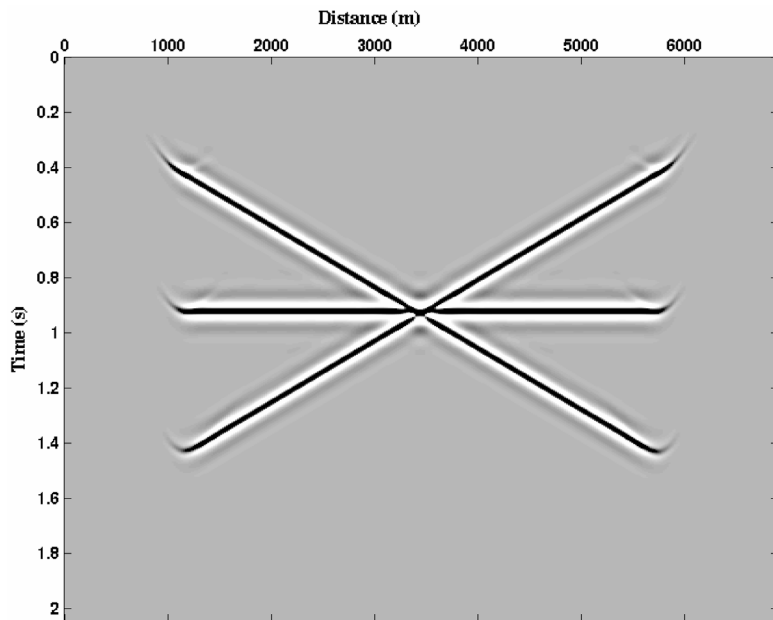


FIG. 6. Extrapolation with the adaptive taper.